



Pergamon

Acta Materialia 50 (2002) 3425–3434



www.actamat-journals.com

Microstrain effect on thermal properties of nanocrystalline Cu

L.H. Qian, S.C. Wang, Y.H. Zhao, K. Lu *

Shenyang National Laboratory for Materials Science, Institute of Metal Research, Chinese Academy of Sciences, 72 Wenhua Road, Shenyang 110016, People's Republic of China

Received 7 January 2002; received in revised form 8 February 2002; accepted 9 April 2002

Abstract

The nanocrystalline (nc) Cu samples with different microstrains but the same grain size were obtained by annealing a magnetron-sputtered nc Cu specimen. Quantitative X-ray diffraction (XRD) measurements show that with an increment of the microstrain from 0.14 to 0.24% the thermal expansion coefficient (TEC) of crystalline lattice increases by about 12%, the static displacement of atom from the equilibrium position (B_S) increases from 0.47 ± 0.09 to $1.16 \pm 0.15 \text{ \AA}^2$, and Debye characteristic temperature (Θ_D) decreases from 307.1 ± 3.1 to 279.2 ± 2.8 K. The microstrain effect on thermal properties in the nc Cu might be attributed to the change in density of grain boundary defects/dislocations. The present investigation demonstrates that the thermal properties of nc materials are determined by not only the grain size but also the microstructure of grain boundaries. © 2002 Acta Materialia Inc. Published by Elsevier Science Ltd. All rights reserved.

Keywords: Magnetron sputtering; X-ray diffraction (XRD); Nanocrystalline copper; Thermal properties

1. Introduction

Studies on thermal properties of nanocrystalline (nc) materials can provide vital information on their intrinsic microstructure characteristics. Many investigations on grain-size dependence of thermal properties in nc materials with a wide range of grain size have been reported [1–4]. These results indicate that thermal properties of nc materials differ evidently from those of their conventional

coarse-grained counterparts due to the large amount of grain boundaries in nc materials.

Klam and his co-workers [1] found that the linear thermal expansion coefficient (TEC) of a polycrystalline Cu with a mean grain size of 17 μm is obviously larger than that of a coarse-grained Cu sample (1.9 mm), indicating that the TEC of grain boundaries is about 2.5–5.0 times that of the corresponding polycrystalline crystalline lattice. Birringer and Gleiter [2] observed that the TEC of an nc Cu with a mean grain size of 8 nm is about 1.94 times that of its conventional polycrystalline counterpart. Lu and Sui [3] noticed that the linear TEC increases markedly with a reduction of the average grain size in porosity-free nc Ni–P samples

* Corresponding author. Fax: 86-24-2399-8660.

E-mail address: lu@imr.ac.cn (K. Lu).

measured by means of thermal–mechanical analysis. Meanwhile, the measurements showed that the TEC enhancement does not follow a simple D^{-1} relationship (D is the mean grain size) as expected from the two-state model of nc materials [5]. Recently, Zhao et al. [4] found that the lattice TEC of ball-milled nc Fe determined by means of quantitative X-ray diffraction (XRD) analysis increases monotonically with a decrease of grain size during the initial stage of ball-milling. But it drops evidently with further milling while grain size remains unchanged. The variation of TEC in the nc Fe specimen is well correlated to the decrease of grain boundary energy as determined by means of thermal analysis. This observation implies that the TEC of crystalline lattice in the nc material may depend not only on the grain size, but also on the grain boundary structure as well.

The Debye–Waller parameter (DWP), $B(T)$, is a measurement of the displacement of atom from the ideal position. It consists of static DWP (B_S) and thermal DWP (B_T). According to the diffraction theory derived by Krivoglas [6], B_S is related to the static displacement of the atom from the equilibrium position caused by defects, such as vacancies, interstitials and dislocations, while B_T is the contribution from the thermal vibrations of the atom around the equilibrium lattice site. The grain-size dependence of $B(T)$ in nc Pd [7–10], Au [11,12], Cr [5], Pb [13] and Se [14] has been investigated. It was found that B_S increases significantly with a reduction of grain size, while B_T shows no or little grain-size dependence in those nc materials. For the nc Cr, the $B(T)$ measured at 20 K increases linearly with the inverse grain size, which is consistent with the two-state model [5]. Therefore, Eastman and Fitzsimmons [5] concluded that an increased B_S is normally attributed to the increased concentration of defects in interface region of the crystalline lattice in nc materials. Ohshima et al. [12] investigated $B(T)$ for ultra-fine Au powders over a temperature range of 112–298 K, and found a large B_S difference from sample to sample even though the grain size of all the three samples is nearly the same of about 10 nm. Harada et al. [11] reported that $B(T)$ for an nc Au does not show a systematic grain-size dependence and ascribed this behavior to the presence of the serious

static lattice strain in the samples. A parameter related to $B(T)$ is the Debye characteristic temperature that designates the cohesion of atoms. Reduced Debye characteristic temperature is frequently observed in nc materials [8–9,14–16].

Meanwhile extensive investigations in the past years indicate a pronounced grain-size dependence on thermal properties of nc materials, other extrinsic factors (such as porosities [17], impurities [18] etc.) as well as intrinsic structural parameters (such as microstrain, grain boundary energy [19]) may also be responsible for the variations of properties. In the present work, the microstrain effect on thermal properties (TEC, DWP, Debye characteristic temperature) in an nc Cu will be investigated experimentally. An obvious microstrain dependence of these thermal properties is detected, that will be discussed in terms of the microstructure characteristics of nc materials.

2. Experimental procedures

Nanocrystalline Cu films were fabricated by means of direct current (DC) magnetron sputtering using a Cu target with a purity of 99.999%. The substrate is selected as silicon (111). The base pressure in the deposition chamber is above 7.0×10^{-5} Pa. The working pressure of pure argon gas is about 1 Pa. Prior to deposition, the target was cleaned for 10 min by sputtering while the substrates were isolated from the plasma by a shutter. The thickness of the as-deposited nc Cu film is about 4 μm determined by means of scanning electron microscopy (SEM) observations. Less than 200 ppm (wt%) oxygen contamination was detected by Auger-electron spectroscopy (AES) on the fresh surface of the as-deposited Cu films.

After being peeled from the Si substrate, the as-deposited nc Cu sample (sample A) was annealed in vacuum (better than 1×10^{-3} Pa) at different temperatures to change its microstrain, 373 K for 10 min (sample B), 373 K for 30 min (sample C) and 383 K for 30 min (sample D), respectively. The coarse-grained Cu powders (with a purity of 99.99% and a mean particle size of about 200 mesh) annealed at 773 K for 4 h was selected as the reference sample (sample E).

XRD measurements of the nc Cu samples were carried out on a Rigaku DMAX/2400 X-ray diffractometer. A rotating Cu target was used with a voltage of 50 kV and a current of 150 mA. The X-ray wavelengths $\lambda_{K\alpha1}$ ($= 1.54056\text{\AA}$) and $\lambda_{K\alpha2}$ ($= 1.544396\text{\AA}$) were selected using a $\langle 0002 \rangle$ graphite crystal scattering at the goniometer receiving slit. The divergence slit angle, scattering slit angle and receiving slit height were selected as 0.5° , 0.5° and 0.15 mm, respectively. The θ – 2θ scans with a step size of $2\theta = 0.02^\circ$ and a fixed counting time of 10 s were made for the nc Cu samples at room temperature ($290 \pm 2\text{K}$). The low temperature XRD experiments were performed on the same diffractometer with a low temperature attachment. The sample was cooled by liquid N_2 through a metal tube and heated by a resistance thread. The temperature was detected by a copper–constantan thermocouple with an accuracy of $\pm 2\text{K}$. In the low temperature experiments (84 – 290 K) only five Bragg reflection peaks (111), (200), (220), (311) and (222) were selected with a step size of $2\theta = 0.02^\circ$ and a count time of 3 s.

Transmission electron microscopy (TEM) experiments were conducted on Philips EM420 microscope with the accelerating voltage of 100 kV. The thin film samples for TEM observations were prepared by means of ion thinning.

3. Results

3.1. Grain size and microstrain

Grain size and microstrain of the nc Cu samples (sample A, B, C and D) were determined by means of XRD measurements. The XRD pattern shows that the measured Bragg reflection profile is a convolution of the functions representing both the instrumental and the physical broadening profile. The instrumental broadening profile is revealed as to be a Gaussian type in the present work by means of a SiO_2 reference sample. After subtracting the instrumental broadening, the physical broadening of Bragg reflection peaks induced by the small grain size (usually represented by a Lorentzian function) and microstrain (Gaussian function) in the measured sample can be obtained. Grain size

and microstrain can be calculated from the XRD results according to Scherrer and Wilson equation [20]

$$\frac{\beta_{hkl}^2}{\text{tg}^2\theta_{hkl}} = \frac{\lambda_{K\alpha1} \beta_{hkl}}{D_{hkl} \text{tg}\theta_{hkl} \sin\theta_{hkl}} + 16 \langle \epsilon_{hkl}^2 \rangle^{1/2}, \quad (1)$$

where λ denotes the wavelength of $CuK_{\alpha1}$ irradiation, D_{hkl} and $\langle \epsilon_{hkl}^2 \rangle^{1/2}$ represent the thickness and the mean lattice strain of the grains in the $\langle hkl \rangle$ direction, respectively. θ_{hkl} is the centroid peak position and β_{hkl} is the integral width of the physical broadening profile. The integral width is

defined by the equation $\beta_{hkl} = 1/I_p \times \int I(2\theta)d\theta$,

where I_p is peak-top intensity and $I(2\theta)$ is intensity at $2\theta_{hkl}$ position. By performing a least-square fit to $\beta_{hkl}^2/\text{tg}^2\theta_{hkl}$ plotted against $\lambda\beta_{hkl}/(\text{tg}\theta_{hkl}\sin\theta_{hkl})$ for all the measured peaks for one sample, the mean grain size D and microstrain $\langle \epsilon^2 \rangle^{1/2}$ are both determined from the slope and the intercept.

Fig. 1 shows the XRD profiles at room temperature for the nc Cu samples. A slight {111} texture exists in the nc Cu samples according to the relative maximum intensity of each Bragg reflection peak. It is obvious that the Bragg reflection peaks for each sample are broadened, which may result from small grain sizes and/or presence of microstrain in the as-deposited and the annealed nc Cu samples. According to Eq. (1), the mean grain

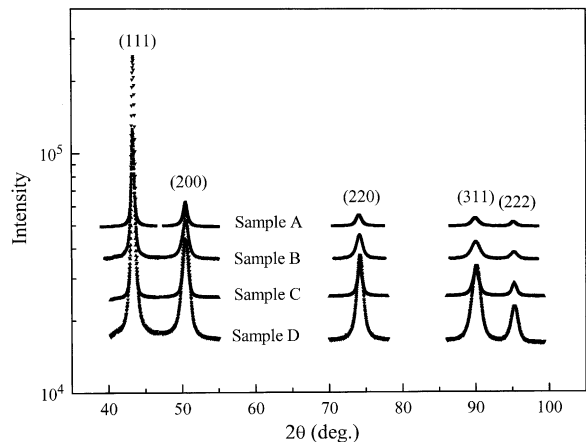


Fig. 1. The XRD profiles at room temperature for the nc Cu samples (sample A, B, C and D).

sizes of sample A, B, C and D, are obtained, being about 10 ± 5 , 10 ± 4 , 10 ± 3 and 12 ± 4 nm, respectively. The mean microstrains in those samples are given as 0.24, 0.21, 0.16 and 0.14%, respectively, as listed in Table 1.

TEM was also employed to determine the grain size and its distribution. Fig. 2 shows the bright-field TEM images for sample A, B, C and D. One can see that each nc Cu sample consists of ultra-fine (in the nm scale) crystallites, which are roughly equiaxed in shape and the grain size distribution is uniform. Some twins can be also found from TEM observations. The selected area electron diffraction (SAED) pattern (as seen in the inset) of the as-deposited nc Cu sample indicates that the crystallographic orientations of the nanocrystallites are random.

Fig. 3 represents the corresponding statistical grain size distribution for the nc Cu samples derived from the bright-field and dark-field TEM images. The peak maximum grain sizes for sample A, B, C and D are 14, 14, 15 and 16 nm, respectively. Although the grain sizes derived from TEM observations differ slightly from those from the XRD analysis, which may originate from the different evaluation principles, a consistent result obtained is that no obvious grain growth occurs during annealing the as-deposited nc Cu sample (sample A, B and C). For sample D, a weak grain growth is observed, and the average grain size is slightly increased, as also detected in XRD analysis (see Table 1).

The above results show that the nc Cu samples with different microstrains but almost the same grain size were obtained by annealing the as-deposited nc Cu sample below 383 K. Our measurement of the thermal stability of the as-deposited nc Cu specimen by using thermal analysis shows that an obvious grain growth occurs at about 420 K, which is agreement with the reported data (400 ~ 450K) in the literature [25]. The remarkable grain-size stability against thermal annealing might be attributed to the narrow grain-size distribution in the present sample, as indicated by Eastman et al. [26].

Thermal annealing below 383 K induced an obvious release in microstrain in the as-deposited nc Cu sample. Or in other words, strain release

occurs prior to grain growth upon annealing in the present sample. This observation is in account with a recent investigation on nc Cu in which a reduction in strain release temperature was observed when the microstrain is larger [19,27]. When the microstrain in the nc Cu was elevated up to 0.15% by cold-rolling, the strain release onsets at about 388 K, which is well below the grain growth temperature in the same sample. For the present as-deposited nc Cu in which microstrain is about 0.24%, the strain release temperature will be even lower (< 373 K) as observed. Similar observations were reported in nc Pd and Ag samples that strain release occurs prior to the grain growth [18].

3.2. Thermal properties

3.2.1. Thermal expansion coefficient

TEC for each sample was calculated according to the lattice parameters determined at different temperatures in an in situ XRD experiment. In order to minimize the calculation error, values of the lattice parameters a for the nc Cu samples at various temperatures (84–290 K) were calculated from the intensity centroid positions of the XRD patterns by using the weighted least-square method. The intensity centroid positions were calibrated by an external standard method using a pure Si polycrystal. The calibration function was expressed as:

$$\Delta 2\theta = \alpha + \beta \cos\theta + \gamma \sin\theta, \quad (2)$$

where α denotes 2θ -axis original displacement, β is related to eccentricity between the sample and goniometer center axis, and γ is related to the sample flatness or absorption. In the experiments, α , β and γ were determined by the least-square method, being $\alpha = 0.017447$, $\beta = 0.063745$ and $\gamma = 0.0082894$. The equation used to calculate lattice parameter is given by:

$$h^2 \frac{a^*}{2} + k^2 \frac{b^*}{2} + l^2 \frac{c^*}{2} + 2kl \frac{b^*c^*}{\cos\alpha^*} + 2lh \frac{a^*c^*}{\cos\beta^*} + 2hk \frac{a^*b^*}{\cos\gamma^*} + E(\theta)x = \frac{4\sin^2\theta}{\lambda^2}, \quad (3)$$

where a^* , b^* , c^* and α^* , β^* , γ^* are the recipro-

Table 1
A list of measured results for various nc Cu samples with different annealing conditions, including the average grain size (D) determined from XRD and TEM observations, the mean microstrain ($\langle \varepsilon^2 \rangle^{1/2}$), the lattice parameter at 290 K (a), the linear TEC in a temperature range of 84 ~ 290K (α_L), the static DWP (B_s), the thermal DWP at 290 K (B_T (290 K)) and Debye characteristic temperature (Θ_D). Results from the literature for the coarse-grained Cu are also included

Sample	Annealing condition	D (nm)	$\langle \varepsilon^2 \rangle^{1/2}$ (%)	a (Å)	α_L (10^{-6} K $^{-1}$) (84–290 K)	B_s (Å 2)	B_T (290 K) (Å 2)	Θ_D (K)
A	As-deposited	10 ± 5	0.242 ± 0.006	3.6161 ± 0.0003	16.56 ± 0.25	1.16 ± 0.15	0.71 ± 0.16	279.2 ± 2.8
B	373 K/10 min	10 ± 4	0.206 ± 0.007	3.6159 ± 0.0005	15.99 ± 0.20	0.81 ± 0.10	0.69 ± 0.12	281.9 ± 2.3
C	373 K/30 min	10 ± 3	0.163 ± 0.005	3.6153 ± 0.0005	15.40 ± 0.18	0.54 ± 0.12	0.66 ± 0.13	285.7 ± 2.1
D	383 K/30 min	12 ± 4	0.141 ± 0.006	3.6147 ± 0.0003	14.96 ± 0.24	0.47 ± 0.09	0.59 ± 0.12	307.1 ± 3.1
E	773 K/40 min	CG powder (200 mesh)	0	3.6149 ± 0.0002	14.14 ± 0.15	0.11 ± 0.08	0.52 ± 0.09	324.4 ± 2.5
F	–	–	0	3.6150 [21] (293 K)	17.0 [22] (293 K)	0.15 [23]	0.44 [23]	320 [24]

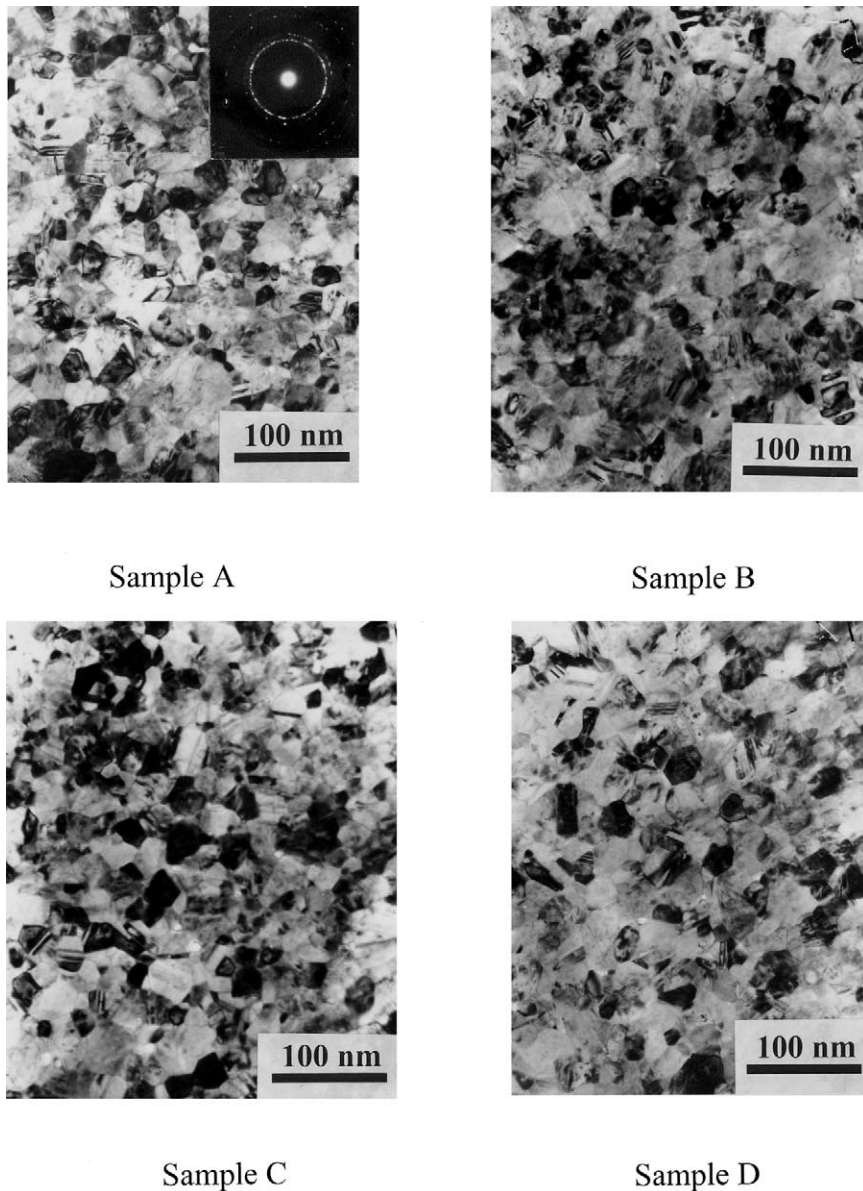


Fig. 2. Bright-field TEM images for sample A, B, C and D, respectively. The inset shows the corresponding selected area electron diffraction (SAED) pattern.

cal-lattice parameters from which the lattice parameter a of nc Cu can be obtained. $E(\theta)$ is the error function that is selected as $\sin^2\theta$ and x is the error weight function.

Fig. 4 shows the temperature dependence of full width of half-maximum (FWHM) for sample A. The FWHM of each Bragg reflection profile hardly

changes with temperature, which indicates that both the average grain size and microstrain do not change within the experimental error when temperature decreases from 290 to 84 K.

Fig. 5 shows the temperature dependence of the lattice parameter a for the as-deposited sample (sample A) and the coarse-grained Cu (sample E).

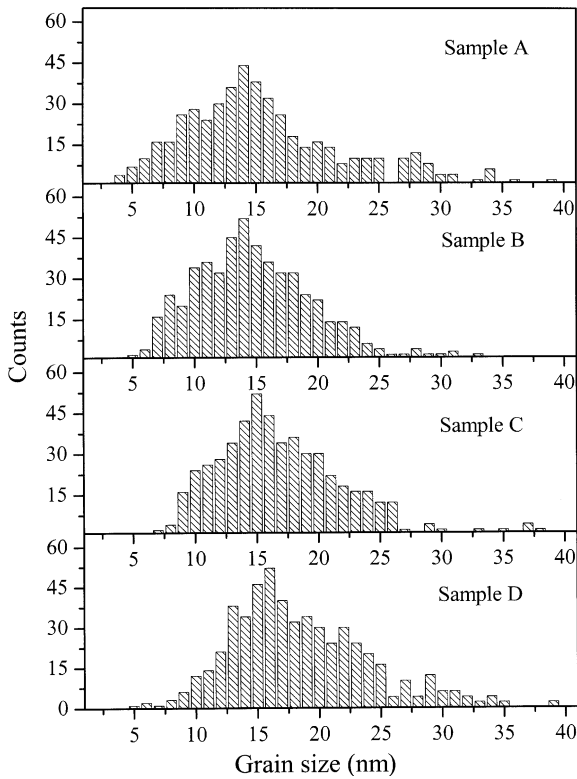


Fig. 3. The grain-size distribution determined from TEM observations for sample A, B, C and D.

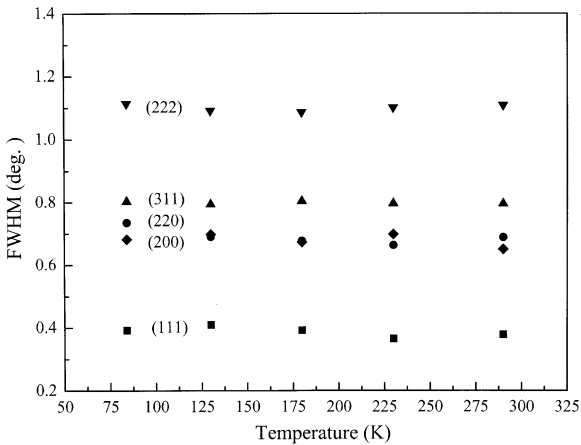


Fig. 4. A plot of FWHM vs temperature for various (hkl) peaks.

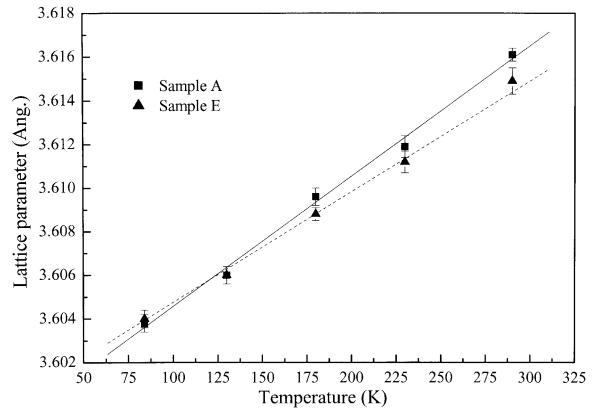


Fig. 5. Temperature dependence of lattice parameter for sample A and E.

It can be seen that the lattice parameter a for both samples increases linearly with temperature. From the least-square fitting to the measured lattice parameter a values, one may derive the TEC values for different nc Cu specimens within this temperature range. For sample A, $\alpha_L = (16.56 \pm 0.25) \times 10^{-6} \text{ K}^{-1}$, and for sample E, $\alpha_L = (14.14 \pm 0.15) \times 10^{-6} \text{ K}^{-1}$.

Fig. 6 shows the variation of α_L against the mean microstrain for the nc Cu samples. The mean α_L in the range of 84–290 K increases approximately linearly from $(14.96 \pm 0.24) \times 10^{-6}$ to $(16.56 \pm 0.25) \times 10^{-6} \text{ K}^{-1}$ with an increment of microstrain from 0.14 to

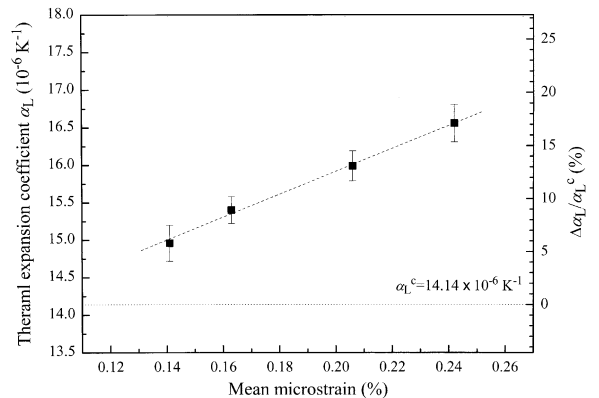


Fig. 6. The variation of TEC (α_L) against the mean microstrain for nc Cu (dash line). The dotted line represents the TEC for the coarse-grained Cu.

0.24%. While the α_L for sample E is $(14.14 \pm 0.15) \times 10^{-6} \text{ K}^{-1}$, which is smaller than that of the other four nc Cu samples. Dilatometric measurements showed that α_L is about $16.8 \times 10^{-6} \text{ K}^{-1}$ for the conventional polycrystalline Cu at 293 K [22], which is little larger than that in the present work. This difference can be attributed to the different measurement techniques and the different temperature ranges. In the dilatometric test, the overall change (including crystalline lattice and grain boundaries) is measured, while in the XRD experiment, only the lattice expansion is considered.

3.2.2. Debye–Waller parameter and Debye characteristic temperature

Atomistic structure information, such as the DWP $B(T)$ and Debye characteristic temperature (Θ_D), can be obtained from the low-temperature XRD experiments. The $B(T)$ for the sample free of texture can be calculated from the XRD patterns by using Warren method [28], which can be expressed as:

$$\ln\left(\frac{\phi_{hkl}}{m_{hkl}}\right) = -2B(T)\left(\frac{\sin\theta}{\lambda}\right)^2 + J, \quad (4)$$

where ϕ_{hkl} is the integrated intensity, m_{hkl} the multiplicity factor, θ_{hkl} the centroid peak position, and J a constant scaled with the incident intensity. The $B(T)$ contains the contributions from the static lattice distortion B_S that are temperature-independent and from the thermal vibrations of atoms B_T , i.e. [28]

$$B(T) = B_S + B_T. \quad (5)$$

For a bulk crystal, temperature-dependent of B_T is known to be well predicted by the Debye approximation, particularly at low temperatures, and the $B(T)$ is used to calculate the Θ_D from expression [28]:

$$B(T) = B_S + \frac{6h^2F(x)}{mk_B\Theta_D}, \quad (6)$$

where h , m , and k_B are the Planck constant, the atomic mass and Boltzmann constant, respectively,

$$x = \Theta_D/T \text{ and } F(x) = \frac{1}{4} + \frac{1}{x^2} \int_0^x \frac{\xi d\xi}{\exp(\xi) - 1}. \quad (7)$$

According to Eq. (4), plotting $\ln(\phi_{hkl}/m_{hkl})$ against $\tau^2(\tau = 4\pi\sin\theta/\lambda)$ for each sample at different temperatures, we can get $B(T)$ at each temperature by least-square fitting to the measured data. By plotting the temperature dependence of $B(T)$ for each sample, $B(T) - T$ can be fitted by adjusting Θ_D and B_S .

The calculated thermal DWP at 290 K, $B_T(290)$, and static DWP, B_S , for both the nc Cu samples and sample E are listed in Table 1. Fig. 7(a) shows the variation of B_S and $B_T(290)$ for the nc Cu samples as a function of the mean microstrain. It is clearly seen that, for the nc Cu samples, B_S increases from 0.47 ± 0.09 to $1.16 \pm 0.15 \text{ \AA}^2$ when the mean microstrain increases from 0.14 to 0.24%, while $B_T(290)$ remains unchanged within the experimental error. For sample E, B_S and $B_T(290)$ are 0.11 ± 0.08 , $0.52 \pm 0.09 \text{ \AA}^2$, respectively.

Fig. 7(b) shows the variation of Θ_D for the nc Cu samples as a function of the mean microstrain.

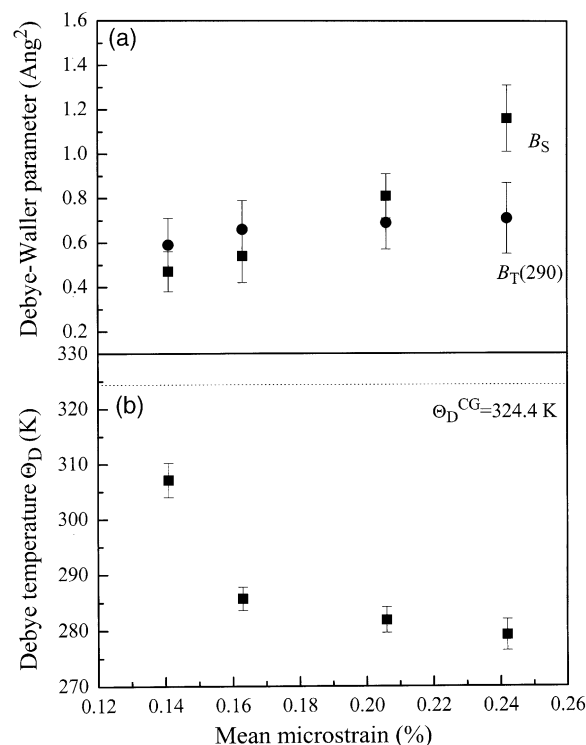


Fig. 7. The variation of B_S , $B_T(290)$ and Debye characteristic temperature (Θ_D) against the mean microstrain for the nc Cu and the coarse-grained Cu (dotted line).

One can see that Θ_D decreases from 307.1 ± 3.1 to 279.2 ± 2.8 K when the mean microstrain increases from 0.14 to 0.24%. These values are smaller than that for sample E ($\Theta_D = 324.4 \pm 2.5$ K) determined in the present work, which is close to the literature data ($\Theta_D = 320$ K) [24]. It is well-known that Θ_D is an essential physical parameter designating the cohesion of atoms. The depressed Θ_D in nc Cu implies a reduction in the cohesion of atoms in the nanometer-sized crystallites, which agrees well with the microstrain dependence of the DWP.

4. Discussion

The experimental data presented above shows an obvious fact that thermal properties (such as TEC, B_S and Θ_D) of the nc Cu are dependent upon microstrain. Basically, microstrain may be attributed to the local deviation of the atom from the equilibrium position in the crystalline lattice, due to the presence of foreign atoms (impurities), porosities, point defects, dislocations or grain boundaries in the sample.

In this work, the effect of contamination and porosity on microstrain can be ruled out for the nc Cu sample as the amount of those is negligible in the as-deposited specimen according to the results of the AES analysis and the TEM observations. And no change in their quantities is expected during thermal annealing of the as-deposited sample. Furthermore, due to the ultra-fine grain, dislocations hardly exist within the crystalline lattice, as observed under TEM and reported in the literature [29]. Consequently, the variation of microstrain may originate primarily from the microstructure change of grain boundaries.

A recent experimental investigation on cold-rolling of an nc Cu sample indicated that microstrain in the nc specimens is closely related to the grain boundary structure [27]. Cold deformation of the nc Cu induced an obvious increment in the microstrain, which is accompanied by an enhanced grain boundary enthalpy and an increased density of grain boundary defects/dislocations. This observation means that microstrain in the nc material is, to some extent, a signature of the density of defects/dislocations within the grain boundaries.

In the present work, a large microstrain in the as-deposited nc Cu sample is detected by quantitative XRD analysis, indicating a high level of defects/dislocations density in grain boundaries. TEM observations showed that most grain boundaries are high-angle ones with large misorientations (Fig. 2), which may originate from the non-equilibrium processing during sputtering deposition. Such a high-energy grain boundary configuration may induce a remarkable deviation of atoms in the vicinity of grain boundaries from their equilibrium lattice positions, resulting in a large microstrain as well as a large mean static displacement of atoms in the crystallites (B_S). When the as-deposited nc sample is annealed, local rearrangements of atoms in grain boundaries take place so that the grain boundary defects/dislocations density is reduced, the overall microstrain in the nanocrystallites is released, too. Therefore, the mean static displacement of atoms is decreased along with an increment of Θ_D , implying atoms in the vicinity of grain boundaries tend to a more equilibrium arrangement.

The observed increase of TEC with a larger microstrain in the nc Cu sample indicated that the thermal expansion coefficient of the nanocrystallites is sensitive to the grain boundary microstructure. With an increase of the grain boundary defect/dislocation density, the TEC of nanocrystallites can be enhanced. This correlation is reasonable as the vibrational properties of atoms are very much depending upon their surrounding coordinations. A larger microstrain with an increased static displacement of atoms in the lattice may result in a larger TEC of the crystallite. This behavior implies that the property variation of nc materials may result from not only the plenty amount of grain boundaries (grain-size effect) but also the property change of the nanocrystallites of which the microstructure is related to the configuration of grain boundaries. In-depth quantitative investigations on the microstructure–property correlations in the nc materials are in progress.

5. Conclusions

Microstrain release without a significant grain growth was observed for the magnetron-sputtered

nc Cu sample annealed below 383 K. It was found that TEC increases from $(14.96 \pm 0.24) \times 10^{-6}$ to $(16.56 \pm 0.25) \times 10^{-6} \text{ K}^{-1}$ with the increment of microstrain from 0.14 to 0.24%. According to the calculated results based on Debye model, the static DWP (B_S) markedly increases from 0.47 ± 0.09 to $1.16 \pm 0.15 \text{ \AA}^2$ with the increment of microstrain, while Θ_D remarkably decreases from 307.1 ± 3.1 to $279.2 \pm 2.8 \text{ K}$. The microstrain effect on thermal properties (including TEC, B_S and Θ_D) for the nc Cu might be related to the variation of defects/dislocations density in grain boundaries. The present investigation demonstrated that thermal properties of nc materials correlate with not only the grain size but also the microstructure of grain boundaries.

Acknowledgements

Financial support from the National Science Foundation of China (Grant No. 50021101), the Ministry of Science and Technology of China (Grant No. 1999064505) and Max-Planck Society of Germany is acknowledged. The authors thank Prof M.L. Sui, Drs W. Wang, L. Zhang, Q.H. Lu, X.J. Gu and J. Zhong for their advice and valuable discussions.

References

- [1] Klam HJ, Hahn H, Gleiter H. *Acta Metall* 1987;35:2101.
- [2] Birringer R, Gleiter H. In: Cahn RW, editor. *Advance in materials science, encyclopedia of materials science and engineering*. Oxford: Pergamon Press; 1988. p. 33-9.
- [3] Lu K, Sui ML. *Acta Metall* 1995;43:3325.
- [4] Zhao YH, Sheng HW, Lu K. *Acta Metall* 2001;49:365.
- [5] Eastman JA, Fitzsimmons MR. *J Appl Phys* 1995;77:522.
- [6] Krivoglaz MA. *Theory of X-ray and thermal-neutron scattering by real crystals*. New York: Plenum Press, 1969.
- [7] Fitzsimmons MR, Eastman JA, Müller-Stach M, Wallner G. *Phys Rev* 1991;B44:2452.
- [8] Eastman JA, Fitzsimmons MR, Thompson LJ. *Philos Mag* 1992;B66:667.
- [9] Ohshima K, Yatsuya S, Harada J. *J Phys Soc Jpn* 1981;50:3071.
- [10] Inagaki M, Sasaki A, Sakai M. *J Mater Sci* 1983;18:1803.
- [11] Harada J, Yao S, Ichimiya A. *J Phys Soc Jpn* 1980;48:1625.
- [12] Ohshima K, Hayashi A, Harada J. *J Phys Soc Jpn* 1980;48:1631.
- [13] Novotny V, Holden TM, Dolling G. *Can J Phys* 1974;52:748.
- [14] Zhao YH, Zhang K, Lu K. *Phys Rev* 1997;B56:14322.
- [15] Kashiwase Y, Nishida I, Kainuma Y, Kimoto K. *J Phys* 1977;C38:C2–57.
- [16] Hong LB, Ahn CC, Fultz B. *J Mater Res* 1995;10:2408.
- [17] Höfler HJ, Averback RS. *Scr Metall Mater* 1990;24:2401.
- [18] Kumpmann A, Günther B, Kunze H-D. *Mater Sci Eng* 1993;A168:165.
- [19] Lu L, Tao NR, Wang LB, Ding BZ, Lu K. *J Appl Phys* 2001;89:6408.
- [20] Klug HP, Alexander LE. In: *Diffraction procedures for polycrystalline and amorphous materials*. 2nd ed. New York: Wiley; 1974. p. 49-1 [chapter 9].
- [21] *Powder Diffraction File*. Joint Committee on Powder Diffraction Standards. Swarthmore, PA, 1990, No. 4-0836.
- [22] William D, Callister JR. *Materials Science and Engineering: An Introduction*. 5th ed. Von Hoffmann Press; 1999, p. 662 [chapter 20].
- [23] Macgillavry CH, Reick GD, editors. *International tables for X-ray crystallography 3*. Dordrecht: Reidel; 1983. p. 23-4 [chapter 3].
- [24] Owen EA, Williams RW. *Proc Roy Soc* 1947;A188:509.
- [25] Huang YK, Menovsky AA, de Boer FR. *Nanostr Mater* 1993;2:587.
- [26] Eastman JA, Liao YX, Narayansamy A, Siegel RW. *Processing Science of Advanced Ceramics, MRS Symposium Proceedings* 1989;155:255.
- [27] Lu L, Sui ML, Lu K. *Acta Metall* 2001;49:4127.
- [28] Warren BE. In: *X-ray diffraction*. Reading, MA: Addison-Wesley; 1969. p. 15-1 [chapter 11].
- [29] Thomas GJ, Siegel RW, Eastman JA. *Scr Metall Mater* 1990;24:201.